

1
2
3
4
5
6
7
8
9
10
11
12
13
14
15
16
17
18
19
20
21
22
23
24
25
26
27
28
29
30
31
32

A three-dimensional finite element analysis of the human hip

Mohammad Akrami ^{a*}, Kim Craig ^a, Mahdieh Dibaj ^a, Akbar A. Javadi ^a, Abdelmalek Benattayallah ^b

^a Department of Engineering, College of Engineering, Mathematics, and Physical Sciences
University of Exeter, Exeter, United Kingdom

^b MR Research Centre, St. Luke's Campus, University of Exeter, Exeter, United Kingdom

*Corresponding Author

Dr Mohammad Akrami

Lecturer in Mechanical Engineering

College of Engineering, Mathematics, and Physical Sciences

University of Exeter

Telephone: 01392 724542

Address: Room 271, Harrison Building, North Park Road, Exeter, Devon, EX4 4QF

Keywords: Finite Element Analysis, Hip biomechanics

Word count:

Submitted as an *Original Article*

33 **Abstract**

34

35 A three-dimensional hip model was created from the MRI scans of one human subject
36 based on constructing the entire pelvis and femur. The ball and socket joint was modelled
37 between the hip's acetabulum and the femoral head to analyse the multiaxial loads
38 applied in the hip joint. The three key ligaments that reinforce the external surface of the
39 hip to help to stabilise the joint were also modelled which are the iliofemoral , the
40 pubofemoral and ischiofemoral ligaments. Each of these ligaments wraps around the
41 joint connection to form a seal over the synovial membrane, a line of attachment around
42 the head of the femur. This model was tested for different loading and boundary
43 conditions to analyse their sensitivities on the cortical and cancellous tissues of the
44 human hip bones. The outcomes of a one-legged stance finite element analysis revealed
45 that the maximum of 0.056 mm displacement occurred. The stress distribution varied
46 across the model which the majority occurring in the cortical femur and dissipating
47 through the cartilage. The maximum stress value occurring in the joint was 110.1 MPa,
48 which appeared at the free end of the proximal femur. This developed finite element
49 model was validated against the literature data to be used as an asset for further research
50 in investigating new methods of total hip arthroplasty, to minimise the recurrence of
51 dislocations and discomfort in the hip joint, as well as increasing the range of movement
52 available to a patient after surgery.

53

54 **1. Introduction**

55

56 The hip joint is one of the most load-bearing joints in the human body and consequently
57 must undergo a large amount of use over a human lifetime. During frequent use, the hip
58 joint can wear down and start to erode; meaning the hip may have to be replaced with a
59 prosthesis. In fact, instances of total hip arthroplasty are performed have increased 40.9%
60 between 1991 and 2005 (1); therefore, the need for more efficient and effective surgery
61 is needed more than ever. As technological and scientific advancements are made,
62 methods of total hip arthroplasty are evolving to improve the range of movement after
63 surgeries and minimise the risk of prosthesis dislocation.

64 Therefore the biomechanical behaviour of the hip joint needs to get investigated to have
65 a better understanding of the related treatments and how different tissues work.
66 Accessing the internal structure of the hip joint in-vivo is impossible to monitor how
67 different segments work and sometimes for measuring the functional behaviours, the soft
68 tissues need to be cut during or before the surgery. Therefore, computational methods
69 are utilised to generate detailed results and analyse the biomechanics of such complex
70 musculoskeletal structure.

71 There are a number of studies that already focus on finite element modelling of the hip,
72 however, many of them analyse hip prostheses (2, 3), or alternatively focus on individual
73 parts of the body like the pelvis (4, 5) or femur (6, 7) without considering their bio-
74 realistic interactions. This main novelty of the current research is modelling both the
75 femur and pelvis in the hip joint besides the cartilage and ligaments. Some of the previous
76 studies modelled the pelvis in half, which the effects of this assumption in terms of the
77 aesthetics have not been investigated in detail. Huiskes & Chao (8) showed an alternative
78 method of finite element analysis on a 2D scale, through superposition of 2D medical
79 images. They analysed the femur under the exertion of a unit force of 1 N applied
80 ellipsoidally over the acetabulum area of the hip joint, creating a simulation of a one-
81 legged stance. This paper measured the critical fracture load of the femur and would be
82 a reasonable study for a project which is limited on resources, like computing power or
83 medical imaging. Keyak et al. (9) used finite element modelling to predict the critical
84 values of femoral load fracture by creating 3D models of 18 pairs of femoral from
85 cadavers.

86 In order to use the computational models for analysing the bio-realistic behaviours,
87 loading and boundary conditions need to be applied precisely. Boundary conditions are
88 proven to present different results depending on the location where the hip joint is fixed.
89 Watson et al. (4), showed that the location of the boundary condition significantly
90 changes the stress distribution and the magnitude of stress across the bones. A 2007 study
91 by Phillips et al. (5) modelled and analysed the hip by setting muscular and ligamentous
92 boundary conditions. This caused the stress distributions around the hip to appear
93 significantly different from that of ordinary fixed boundary conditions. Throughout the
94 literature, mostly the pubic symphysis is fixed as the main boundary condition. Another
95 study compared deformation under loading by modelling the pubic symphysis as both a

96 rigid and deformable boundary condition (7). Both approaches showed similar pressures
97 and stresses, however, the rigid model showed high stresses in the cancellous sections of
98 the inferior pubis bone and the superior dome. Phillips, et al. (5) also considered the
99 different options when modelling the pubic symphysis, but ultimately decided that rigid
100 modelling is more practical when focussing on the strength of the hip joint itself in order
101 to decrease the computational cost. There were several assumptions made in previous
102 studies that should be assessed, the first, a common one, was to assume the perfect
103 spherical shape of the femoral head and the corresponding acetabular socket (5).
104 However, this assumption is disputed and unrealistic; the femur head is known to have a
105 concave depression within it named the fovea capitis, which is the location where one of
106 the ligaments in the hip attaches to the femur. Also, previous studies neglect the effect
107 of changed in the shape of the femoral head and cartilage thickness due to joint
108 degeneration which may have significant effect on stress distribution (10). In addition
109 to this, several papers assume unique values for the thickness of cartilage and cancellous
110 bones (11, 12). The frictionless surface-to-surface interaction was applied in studies in
111 which the effects of the frictionless assumption has not been investigated in detail (13).
112 Therefore, the main purpose of this study is to determine the biomechanical properties
113 of the hip joint during different types of loading and how these will cause the functional
114 parameters of the cortical and cancellous bones of the hip joint for increase-decreasing
115 the loads. This can help to understand the roles of these bones in everyday locomotion
116 patterns.

117

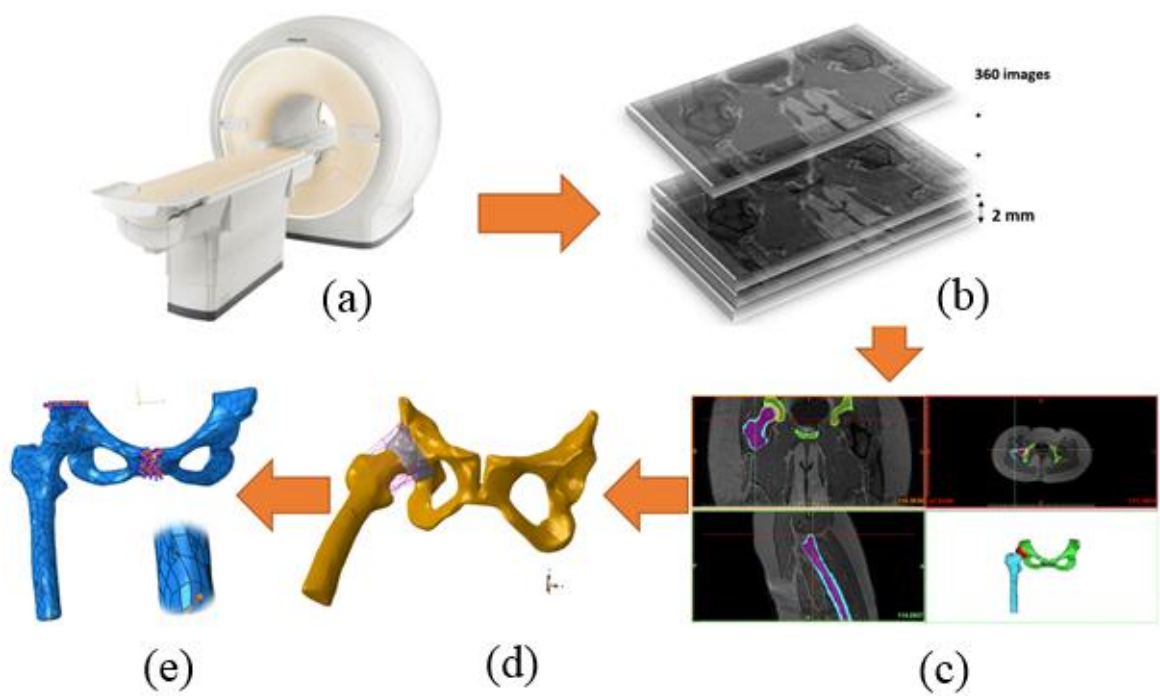
118 **2. Methods and materials**

119 **2.1. Medical image analysis**

120

121 Three-dimensional versatile geometries of the current hip model were reconstructed from
122 the medical MRI data. The MRI scanning was performed on a 1.5 Tesla Phillips Intera
123 system using T1 3D Gradient Echo sequence (TR/TE = 57 ms/21 ms, flip angle 90°, 360°
124 slices and spatial resolution with voxels size of $0.5 \times 0.5 \times 0.5 \text{ mm}^3$). The geometries
125 were captured by scanning the right hip of a healthy female subject (20 years old, with
126 no history of upper limb injuries or hand abnormalities) in the neutral position with a 2

127 mm slice interval. All the images were segmented manually to reconstruct the boundaries
 128 of bones and soft tissues using ScanIP software (Synopsys, Mountain View, USA).
 129 Automatic smoothing was carried out in order to omit the rough surfaces and sharp
 130 edges; thereby a surface made from the average nodal positions was produced, which
 131 more accurately represented bone geometry. Cancellous and cortical tissues of the femur
 132 and the whole structure of the pelvis have been modelled to have a three-dimensional
 133 structure of its anatomy (14). In order to model the articulations between the two bones,
 134 cartilage layers were designed. There are two key areas of cartilage in the hip, both found
 135 in the articular joint section; the first is on the head of the femur and the second in the
 136 pelvic acetabulum. Cartilage that appears on articular surfaces like the hip is hyaline
 137 cartilage; which providing a smooth lubricated surface for joints as well as supporting
 138 soft tissues. In this study, the cartilage layers on the surface of the acetabulum and
 139 femoral head were reconstructed based on the MRI data to maintain their bio realistic
 140 structure. So far, based on the knowledge of authors, there is no study which has designed
 141 the cartilage topological structures for the hip joint based on the bio-realistic image-
 142 driven data.
 143



144
 145 **Figure 1** Developing process of the human hip model: (a) Scanning the subject (b) Generating DICOM files (c)
 146 medical image processing to segment the bones and cartilages (d) adding ligaments to the model in SOLIDWORKS
 147 (e) applying loads and boundary conditions to the finite element model in ABAQUS

148 **2.2. Finite element modelling**

149 After the medical image data were processed using medical image processor software
 150 (ScanIP), the STL format files were transferred to Solidworks software (Dassault
 151 Systèmes, SolidWorks Corp., USA) to assign the boundary surfaces and assembling the
 152 solid models for the bones and the designed soft tissues based on Bio-CAD Image-Based
 153 technique (15). The whole pelvis was designed besides the femur which was designed
 154 partially to analyse the hip joint. These two bony tissues were divided into cortical and
 155 cancellous to have the bio-realistic representations of this anatomical structure. The
 156 material properties derived from literature by distinguishing the cortical and cancellous
 157 properties for the hard tissues (See Table 1). For the ligaments, the stiffness values are
 158 assigned in detail from the literature (See Table 2). Each springs' stiffness was calculated
 159 using the parallel springs rule. The total stiffness of a group of parallel springs is the sum
 160 of each springs' individual stiffness. The material properties and element types used for
 161 modelling different components of the hand complex are listed in detail in Table 1. The
 162 mesh sensitivity study was applied through the convergence analysis by the gradual
 163 increase of the mesh quality until deviations in the evaluated stresses reached <5% (16).

164 **Table 1** Material properties and element types of the human hip finite element model
 165

Components	Materials	Element types	Young's modulus (MPa)	Poisson's ratio	References
Cortical bone	Solid, linear elastic	Tetrahedral	17000	0.3	(4, 11, 13, 17-19)
Cancellous bone	Solid, linear elastic	Tetrahedral	70	0.2	(13)
Cartilage	Solid, linear elastic	Tetrahedral	15	0.45	(7, 13)

166

167

Table 2 Ligament properties for the hip joint ligaments (13)

Ligament	Ligament Stiffness (N/m)	Number of Spring elements
Teres	68000	1
Ischiofemoral	39600	10
Pubofemoral	36900	6
Inferior Iliofemoral	100700	4
Superior Iliofemoral	97800	4

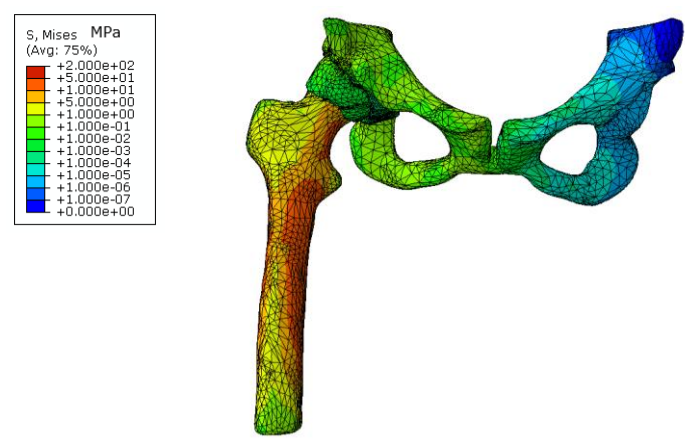
168 The cortexes and pubic symphysis were fixed throughout the analyses. A force of 600 N
169 applied perpendicularly to the acetabulum at the end of the femur length to recreate a
170 one-legged stance (5). Constraints and interactions were added to the model to ensure
171 that each of the components in the model reacts with each other accurately. A frictionless
172 surface-to-surface interaction was created between the surfaces of the cartilage and
173 bones; between the hip and femur cartilage free movement was allowed, however
174 between bone and cartilage for both the hip and the femur a “tie” constraint was used to
175 fix the surfaces together (20).

176

177 3. Results

178

179 Loading values were captured from literature (5, 11) in order to compare the results for
180 the validation process. Furthermore, the addition of cartilage and ligaments to the model
181 altered the results away from those previously presented, especially due to different
182 material properties or geometry. Higher stresses on the femur within the loading plane
183 were predicted (see figure 2), as these were expected due to the bending applied to the
184 femur in this direction. The maximum stress occurred in the cortical femur was close to
185 75 MPa, which is similar to the reported 70 MPa (5).

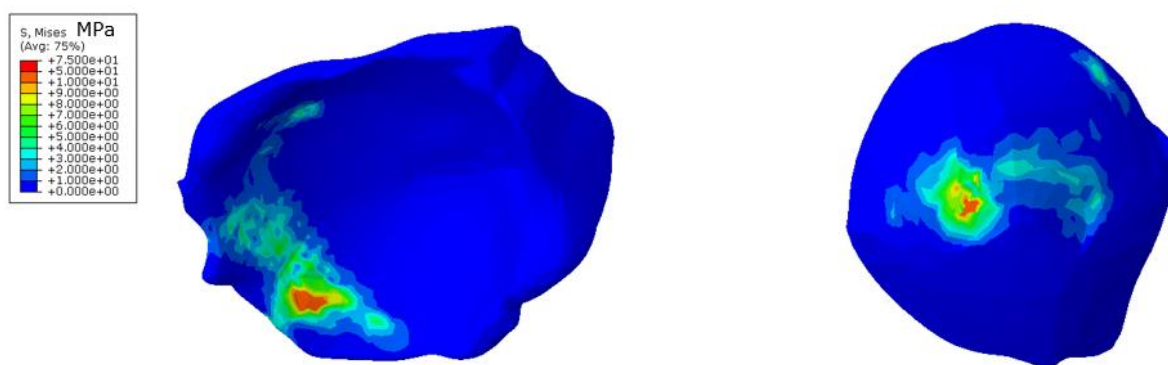


186 **Figure 2:** Stress distribution within the bones and cartilage layers in normal standing condition

187

188 It can be interpreted that most of the weight from the upper body is supported in the legs
189 rather than the pelvis and lower spine. The cortical proximal femur sustained the highest
190 stress values of any component in the hip joint. Both cancellous bones show lower values
191 of stresses as it was expected (21). The cancellous pelvic bone had a maximum stress of

192 0.1827 MPa, while the cancellous femur had a maximum stress of 12.42 MPa which
 193 shows the role of the femur in sustaining the loads before transmitting to the knee and
 194 ankle joints. The maximum stress occurring in the cancellous femur was on the femoral
 195 head; while the cortical femur had a high amount of stress at this point as well since this
 196 was where the Teres ligament was located. The cortical pelvic bone presented a
 197 maximum stress of 9.581 MPa around the acetabulum. Regarding the cartilage, they
 198 sustain most of the stresses in the contact region. The femur and pelvic cartilage each
 199 had a maximum stress of 31.95 MPa and 13.7 MPa, respectively. The stress plot for the
 200 cartilage shows medium to high stresses in the direction of the femur's rotation, while
 201 other areas showed arbitrary locations stress (see Figure 3).



202
 203 **Figure 3** Stress distributions of the pelvic cartilage (left) and femur cartilage (right)
 204

205 The dissipation of stress throughout the joint from the point of contact revealed that the
 206 stress from a standing load is not very widespread, since the majority of the force was
 207 distributed on the femoral head, revealing that frequent use and high loads concentrated
 208 on a small part of the body would eventually cause failure risks, especially in the elderly
 209 people which the cortical tissues are thinning (22) . This also reveals that a large majority
 210 of the hip joint, especially the pelvis, exists for the protection of internal organs rather
 211 than for structural integrity in supporting the body. Other loading conditions may present
 212 alternative results in the overall structural stresses, for example, a large amount of the
 213 pelvis experienced little to no stress, alternative loading and boundary conditions around
 214 these areas could produce differing results; however, the hip joint is more commonly
 215 under stresses during walking or standing (the current loading), which may explain why
 216 falls are more likely to cause a hip dislocation or injury (9) due to higher magnitude and
 217 multi-directional forces causing high stresses in commonly low-stress areas, which the

218 hip joint may not be equipped for. The ligaments experienced the majority extension in
 219 the plane of rotation of the femur with the maximum strain in the model was 0.009543%.
 220 The maximum deformation under standard loading is 0.05648 mm. As expected, the
 221 deformation was the smallest close to the centre of the joint rotation and increases away
 222 from this point, this is the natural movement of the femur about the joint.

223

224 **4. Discussions**

225 By running the model for 10% and 20% above and below the standard load, the load
 226 sensitivity was analysed (See figures 4 and 5). The results show that the strain or
 227 deformation changes more than the stress while the loads are increased/decreased. This
 228 means most of the excess energy from extra loads can get dissipated in the cartilage
 229 layers while the bones are articulating (Figure 4).

230

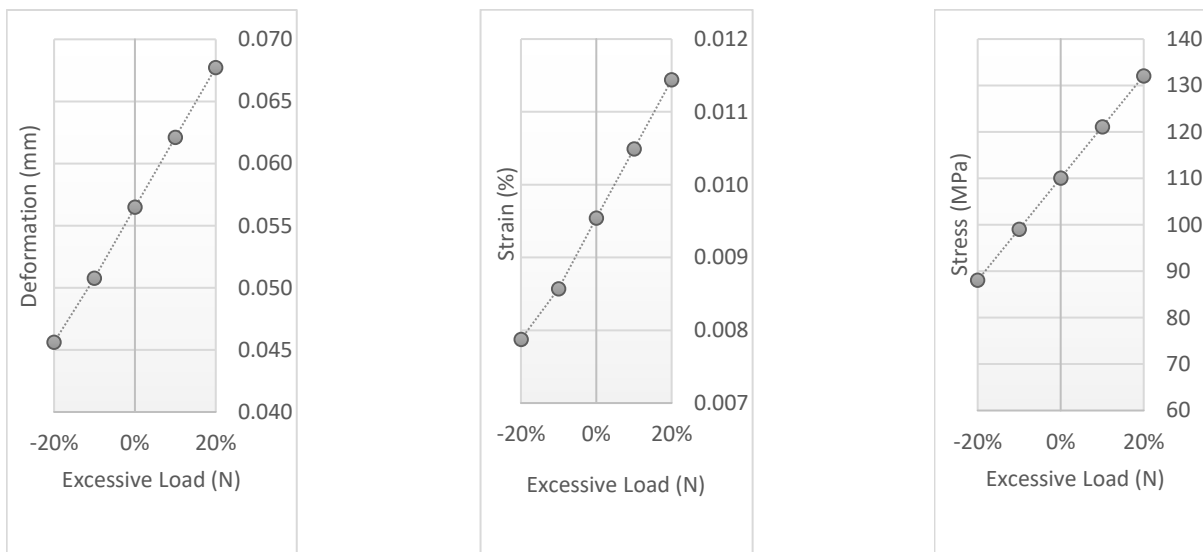
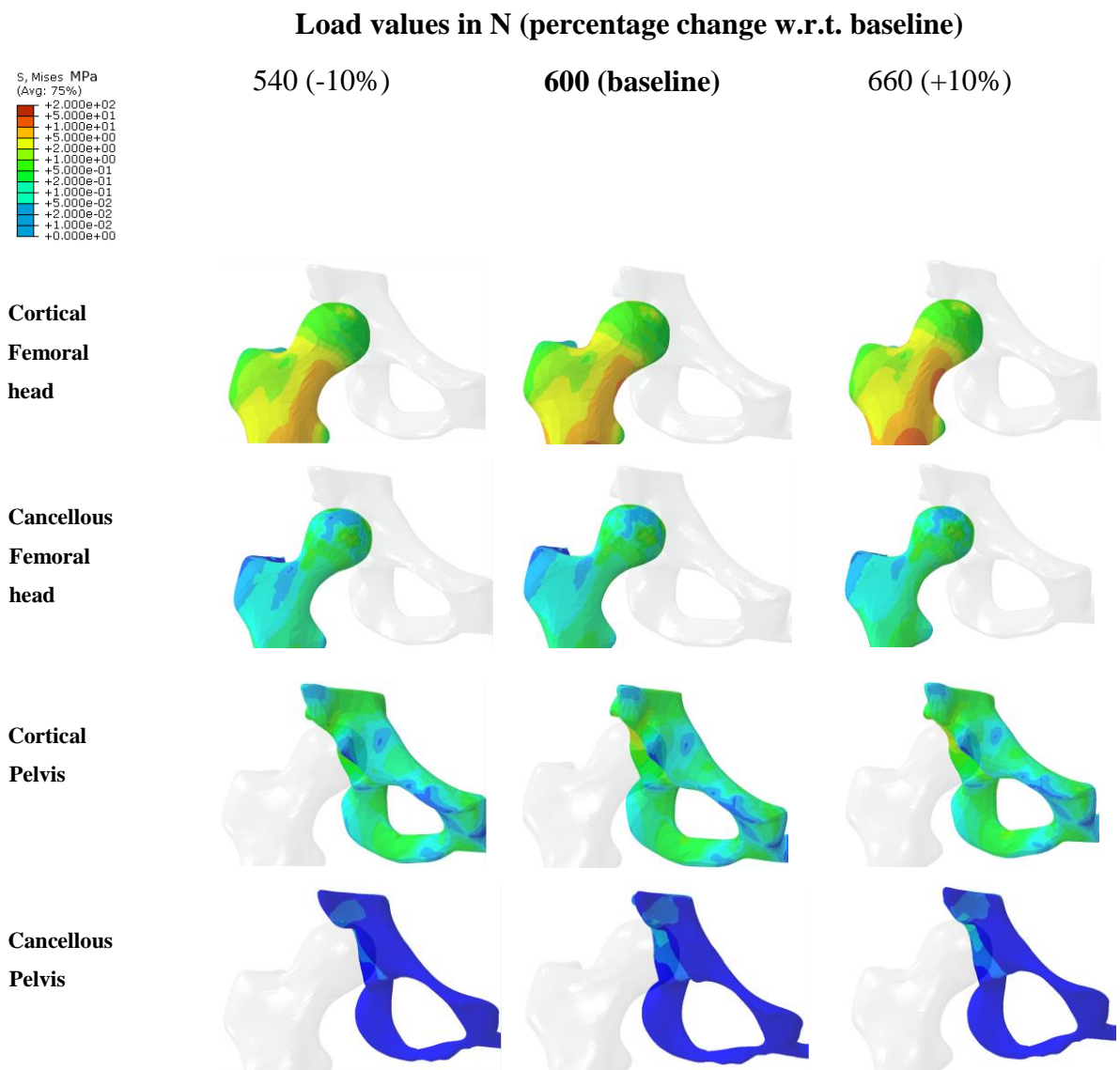


Figure 4: Functional parameters of the hip bones for increase-decreasing the loads

231

232 When the loads were applied, the stress is not evenly distributed within the different bony
 233 tissues (See figure 5). The cortical femoral head sustained more stresses comparing with
 234 the spongy cancellous to stabilise the body during different daily activities. While the
 235 load is being increased by 10%, excessive stresses are then localised on the femur neck
 236 which causes fracture risks as the intertrochanteric areas are releasing some of these
 237 stresses and therefore the extra energy is merely sustained by the femoral head. Less

238 stress was observed around the ventrocranial region of the acetabulum and ventrolateral
 239 of the head as the cartilage is thicker (23). Though some studies (24, 25) show there is
 240 no correlation between aggregate modulus of articular cartilage and its thickness (26),
 241 thicker cartilage retains more excessive energy to reduce the effects of sudden shocks.
 242 For the normal pressures, the stresses were evenly distributed between the acetabulum
 243 and the acetabular cartilage to maintain the existed solidarity between the head of the
 244 femur and the acetabulum.
 245



246 **Figure 5** Stress distributions of the cancellous and cortical femur and pelvis bones by different loading values
 247

248 **5. Conclusion**

249

250 This model predicted how the loads are distributed within the different tissues of the hip
251 bones and interconnected tissues. The model predicted the excessive loads will have
252 more stress concentration around the femur neck which cause can cause fracture in these
253 regions. Less stress was observed around the ventrocranical region of the acetabulum
254 and ventrolateral of the head.

255 This developed model can be used as an asset to understand the effects of sudden
256 excessive loads lead to the hip dislocations so the stress patterns after such injuries can
257 be compared against the healthy cases, for the surgical or treatment planning. The
258 constructed FE model of the hip can improve our understanding of this major
259 musculoskeletal complex.

260 Several limitations exist when developing such kinds of computational FE models.
261 Firstly these kinds of computational models are designed on a subject-specific basis;
262 therefore increasing the number of participants would be valuable to complement the
263 results. The second limitation is better to design the ligaments in three dimensions rather
264 than spring elements, however, in this study, the ligaments origin and insertion were
265 enigmatic in the MRI data and therefore simplifications have been made for representing
266 these. Although the model was validated, replacing the ligaments in three-dimensional
267 structures can improve our understanding of their roles.

268

269 **Acknowledgement**

270 The authors would like to thank Christina Doyle and Andrew John Timperley for the
271 knowledge and resources they provided, which helped define the project. Also, we
272 appreciate the “Simpleware software solutions” for providing the ScanIP software,
273 especially Philippe Young for all his support. Also, we thank the anonymous reviewers
274 for their insightful comments and suggestions.

275

276 **Competing interests**

277 None declared

278 **Funding**

279 None

280 **Ethical approval**

281 Approved by the CEMPS ethics committee, University of Exeter, with the reference
282 number: eEMPS000040 v3.0.

283

284 **References**

- 285 1. Cram P, Lu X, Callaghan JJ, Vaughan-Sarrazin MS, Cai X, Li Y. Long-term
286 trends in hip arthroplasty use and volume. *The Journal of arthroplasty*. 2012;27(2):278-
287 85. e2.
- 288 2. Levadnyi I, Awrejcewicz J, Gubaua JE, Pereira JT. Numerical evaluation of bone
289 remodelling and adaptation considering different hip prosthesis designs. *Clinical*
290 *Biomechanics*. 2017;50:122-9.
- 291 3. Watanabe Y, Shiba N, Matsuo S, Higuchi F, Tagawa Y, Inoue A. Biomechanical
292 study of the resurfacing hip arthroplasty: finite element analysis of the femoral
293 component. *The Journal of arthroplasty*. 2000;15(4):505-11.
- 294 4. Watson PJ, Dostanpor A, Fagan MJ, Dobson CA. The effect of boundary
295 constraints on finite element modelling of the human pelvis. *Medical engineering &*
296 *physics*. 2017;43:48-57.
- 297 5. Phillips A, Pankaj P, Howie C, Usmani A, Simpson A. Finite element modelling
298 of the pelvis: inclusion of muscular and ligamentous boundary conditions. *Medical*
299 *engineering & physics*. 2007;29(7):739-48.
- 300 6. Rüdiger HA, Parvex V, Terrier A. Impact of the femoral head position on moment
301 arms in total hip arthroplasty: a parametric finite element study. *The Journal of*
302 *arthroplasty*. 2016;31(3):715-20.
- 303 7. Rapperport D, Carter D, Schurman D. Contact finite element stress analysis of
304 the hip joint. *Journal of orthopaedic research*. 1985;3(4):435-46.
- 305 8. Huiskes R, Chao E. A survey of finite element analysis in orthopedic
306 biomechanics: the first decade. *Journal of biomechanics*. 1983;16(6):385-409.
- 307 9. Keyak JH, Rossi SA, Jones KA, Skinner HB. Prediction of femoral fracture load
308 using automated finite element modeling. *Journal of biomechanics*. 1997;31(2):125-33.
- 309 10. Kempson G, Spivey C, Swanson S, Freeman M. Patterns of cartilage stiffness on
310 normal and degenerate human femoral heads. *Journal of Biomechanics*. 1971;4(6):597-
311 609.
- 312 11. Anderson AE, Peters CL, Tuttle BD, Weiss JA. Subject-specific finite element
313 model of the pelvis: development, validation and sensitivity studies. *Journal of*
314 *biomechanical engineering*. 2005;127(3):364-73.
- 315 12. Henak CR, Ateshian GA, Weiss JA. Finite element prediction of transchondral
316 stress and strain in the human hip. *Journal of biomechanical engineering*.
317 2014;136(2):021021.
- 318 13. Zou Z, Chávez-Arreola A, Mandal P, Board TN, Alonso-Rasgado T.
319 Optimization of the position of the acetabulum in a ganz periacetabular osteotomy by
320 finite element analysis. *Journal of Orthopaedic Research*. 2013;31(3):472-9.
- 321 14. Starly B, Fang Z, Sun W, Shokoufandeh A, Regli W. Three-dimensional
322 reconstruction for medical-CAD modeling. *Computer-Aided Design and Applications*.
323 2005;2(1-4):431-8.
- 324 15. Sun W, Starly B, Nam J, Darling A. Bio-CAD modeling and its applications in
325 computer-aided tissue engineering. *Computer-aided design*. 2005;37(11):1097-114.
- 326 16. Akrami M, Qian Z, Zou Z, Howard D, Nester CJ, Ren L. Subject-specific finite
327 element modelling of the human foot complex during walking: sensitivity analysis of

328 material properties, boundary and loading conditions. *Biomechanics and modeling in*
329 *mechanobiology*. 2018;17(2):559-76.

330 17. Sun J, Yan S, Jiang Y, Wong DW-c, Zhang M, Zeng J, et al. Finite element
331 analysis of the valgus knee joint of an obese child. *Biomedical engineering online*.
332 2016;15(2):158.

333 18. Cruz D J, Rasgado MT A, CG B. Failure Analysis Following Osteochondroplasty
334 for Hip Impingement in Osteoporotic and Non-Osteoporotic Bones. *Journal of*
335 *Osteoporosis and Physical Activity*. 2016.

336 19. Alonso-Rasgado T, Jimenez-Cruz D, Bailey CG, Mandal P, Board T. Changes in
337 the stress in the femoral head neck junction after osteochondroplasty for hip
338 impingement: a finite element study. *Journal of Orthopaedic Research*.
339 2012;30(12):1999-2006.

340 20. Fan N, Chen G. Numerical study of squeaking suppresses for ceramic-on-ceramic
341 hip endoprosthesis. *Tribology International*. 2012;48:172-81.

342 21. Bayraktar HH, Morgan EF, Niebur GL, Morris GE, Wong EK, Keaveny TM.
343 Comparison of the elastic and yield properties of human femoral trabecular and cortical
344 bone tissue. *Journal of biomechanics*. 2004;37(1):27-35.

345 22. Engelke K, Prevrhal S, Genant HK. Macro-and microimaging of bone
346 architecture. *Principles of Bone Biology (Third Edition)*: Elsevier; 2008. p. 1905-42.

347 23. Kurrat HJ, Oberländer W. The thickness of the cartilage in the hip joint. *Journal*
348 *of anatomy*. 1978;126(Pt 1):145.

349 24. Athanasiou K, Rosenwasser M, Buckwalter J, Malinin T, Mow V. Interspecies
350 comparisons of in situ intrinsic mechanical properties of distal femoral cartilage. *Journal*
351 *of Orthopaedic Research*. 1991;9(3):330-40.

352 25. Athanasiou K, Agarwal A, Dzida F. Comparative study of the intrinsic
353 mechanical properties of the human acetabular and femoral head cartilage. *Journal of*
354 *Orthopaedic Research*. 1994;12(3):340-9.

355 26. Shepherd D, Seedhom B. Thickness of human articular cartilage in joints of the
356 lower limb. *Annals of the rheumatic diseases*. 1999;58(1):27-34.

357